Online Detection of Fundamental and Interharmonics in AC Mains for Parallel Operation of Multiple Grid-Connected Power Converters

Boli Chen, *Member, IEEE*, Gilberto Pin, Wai Man Ng, *Member, IEEE*, Peng Li, Thomas Parisini, *Fellow, IEEE*, and Shu-Yuen Ron Hui, *Fellow, IEEE*

***Abstract*—Parallel operation of multiple grid-connected power converters through *LCL* filters is known to have the potential problem of triggering oscillations in the ac mains. Such oscillatory frequencies are not integral multiples of the fundamental frequency and, hence, form a new source of interharmonics. Early detection of such oscillations is essential for the parallel power converters to move out of the unstable zone. This paper presents an online observer-based algorithm that can perform fast detection of interharmonics within a specified frequency band. The algorithm has been adopted in a specific and reduced form from an integral observer algorithm for detection of fundamental and interharmonic voltage components in the ac mains. A new method based on the kernel signal for fast interharmonic detection is proposed and practically verified. It has been implemented in a digital controller to detect oscillations such as those occurring between two grid-connected power converters. The practical results indicate that the algorithm can locate such frequency within the specific frequency band within one mains cycle.**

***Index Terms*—Active power filters, fundamental extraction, harmonics detection, interharmonics detection.**

I. Introduction

THE tsunami and the subsequent disaster in Fukushima nuclear power facilities in March 2011 have prompted some countries such as Germany to speed up the deployment of distributed renewable energy sources such as wind and solar energy. On the domestic level, rooftop photovoltaic (PV) systems have been increasingly installed in the distribution networks. Unlike traditional fossil-fuel-based power generation, distributed renewable generation systems are usually bidirectional. For example, solar power generated by the PV systems can be consumed by domestic loads, while surplus power can be injected into the power supply side (i.e., the distribution networks).

Renewable energy sources are connected to the distribution networks through power electronics circuits such as bidirectional power inverters [1]. Grid-connected inverters are usually connected to the ac mains through *LCL* filters [2]. Increasing use of grid-connected PV inverters pose new technical challenges. Reports over the last two decades indicate that parallel operations of multiple grid-connected inverters could trigger resonance among their *LCL* filters [3]–[7]. Such resonance could result in not only voltage oscillations in the ac mains, but also system instability because the grid-connected inverter requires the mains voltage waveform for synchronization in the control loop. Recently, the resonance characteristics and stability problem caused by the interactions of multiple parallel *LCL*-filtered inverters has been reported in [8]. If resonance occurs, the control systems of the parallel power inverters should move their operating points out of the unstable zones. An alternative approach is to use active damping circuits to damp down the oscillations [9], [10].

Because grid-connected power inverters are power electronics circuits that require the information of the mains voltage, early and fast detection of such resonance is paramount in stability control of the parallel inverters. The challenge in this project lies with the nature of this type of oscillations, because the *LCL* filter parameters may vary from one manufacturer to another. The oscillatory frequencies are not identical in all situations and these frequencies are not integral numbers of the fundamental frequency. In other words, these oscillatory voltage components are 'interharmonics." Such interharmonics tend to fall within a certain frequency band that depends on the switching frequency of the inverters and the parameters of the *LCL* filters. In [11] and [12], the interharmonics are in the range of about 1.7–2.0 kHz.

The presence of interharmonics makes it difficult to model and detect the frequency components in the power system signals [26]. Conventionally, the discrete Fourier transform (DFT) and its many variants [15]–[19] are preferred for the efficiency

Manuscript received April 6, 2017; revised July 3, 2017, September 6, 2017, and November 5, 2017; accepted December 11, 2017. Date of publication January 3, 2018; date of current version August 7, 2018. This work was supported in part by the Hong Kong Research Council under the Theme-Based Research Fund T23-701/14-N, and in part by the European Union's Horizon 2020 research and innovation programme (KIOS CoE) under Grant 739551. Recommended for publication by Associate Editor Y. Xue. *(Corresponding author: Shu-Yuen Ron Hui.)*

B. Chen and P. Li are with the Department of Electrical and Electronic Engineering, Imperial College London, London SW7 2AZ, U.K. (e-mail: boli.chen10@imperial.ac.uk; peng.li13@imperial.ac.uk).

T. Parisini is with the Department of Electrical and Electronic Engineering, Imperial College London, London SW7 2AZ, U.K., with the Department of Engineering and Architecture, University of Trieste, TS 34127, Italy, and also with the KIOS Research and Innovation Center of Excellence, University of Cyprus, Nicosia 1678, Cyprus (e-mail: t.parisini@imperial.ac.uk).

G. Pin is with Electrolux, Porcia 33080, Italy (e-mail: gilbertopin@alice.it).

W. M. Ng is with the Department of Electrical and Electronic Engineering, The University of Hong Kong, Hong Kong (e-mail: wmng@eee.hku.hk).

S.-Y. R. Hui is with the Department of Electrical and Electronic Engineering, The University of Hong Kong, Hong Kong, and also with Imperial College London, London SW7 2AZ, U.K. (e-mail: ronhui@eee.hku.hk).

Color versions of one or more of the figures in this paper are available online at http://ieeexplore.ieee.org.

Digital Object Identifier 10.1109/TPEL.2017.2789303

in stationary conditions (i.e., when the frequency content is constant within the considered time window) and for their computational efficiency. In [14], the DFT is expressed in a matrix-vector formulation leading to a variant of traditional approach for computational savings. Such technique is also referred to as the modified harmonic domain [18]. From the practical perspective, some issues can be caused by improper application of DFT (e.g., asynchronous sampling) [26], including an aliasing effect, spectral leakage, and picket-fence effect. In [13], the leakage effect is addressed by adaptively adjusting the window width for DFT. An alternative solution is proposed in [16] aiming at restoring the spectral leakage energy. It is shown that the inherent errors due to the leakage effects consisting in measurement devices can be fixed by this recursive group harmonic power minimizing strategy. On the other hand, the picket-fence effect is dealt with in [27] by an FT-based approach with interpolatory polynomial approximation for waveform reconstruction. Very recently, a multiple interharmonics spectrum separation algorithm is proposed to distinguish intensive interharmonics in the case the signal is asynchronously sampled [33]. Apart from the DFT, the ESPRIT and Prony-based methods represent valid alternatives within the frequency domain but offers high-frequency-resolution DFT at the price of more computational requirements [14]. The subspace least mean square method is recently proposed in [30] for highly accurate estimation of interharmonics under a noisy environment with a data sampling window of 1/30 s only. Due to the complexity, high-resolution methods are suitable only for offline analysis and benchmark. Another significant category of interharmonic detection methods involves the adaptive signal processing techniques based on a filter bank with adaptive parameter estimation in the time domain rather than the frequency domain [29]. More specifically, by linking *n* phase-locked loop (PLL) units within one "external" loop, the architecture devised in [20] succeeds in extracting the harmonics and interharmonics from a multisinusoidal measurement. The multi-PLL scheme is then enhanced by incorporating downsampler for each PLL unit to reduce the computational effort of the overall estimator [28]. By replacing the PLLs with a bank of adaptive notch filters (ANF), a new scheme is developed in [21] showing advantages from a computational perspective in comparison with the PLL counterpart reported in [20]. Noticeably, because of the unknown initial conditions, the adaptive approaches (i.e., PLL and ANF) have slower dynamic response compared to DFT despite the merit in terms of robustness and ease of frequency additivity. Detailed comparison of commonly used interharmonic detection techniques is performed in [32]. In practice, the field programmable gate array architectures offer a very cost effective solution for implementing a complicated algorithm for harmonic and interharmonics monitoring [31].

With the aim of improving the convergence speed of a time-domain method without significantly increasing the computation burden, a novel kind of kernel-based algorithms has been recently proposed for estimating *n* sinusoidal components with arbitrary frequencies [22]. This class of algorithms has been adopted for fast detection of fundamental and harmonics for grid-connected power electronics equipment [23]. The basic theory is based on a rather complex mathematical framework, which is beyond the scope of this paper. While the original algorithm can estimate multiple frequency components including the fundamental, harmonics, and interharmonics, the objective of this paper is to adopt this theory in a specific form to explore the use of this estimator for fast and accurate tracking of the fundamental and a single interharmonic within specified frequency band in the ac mains. Practical results are included to verify the feasibility and fast response of the proposed method.

II. Problem Statement and Preliminaries

In this section, the generic algorithm for fast detection of signals of n (arbitrary) frequencies is introduced. Equations (1)–(20) are used to explain the general concept of multiple frequency detection in Sections II and III. Then, the estimator will be adopted for the specific application and the implementation of tracking the fundamental and an interharmonic (which is far from the fundamental frequency and is not an integral multiple of the fundamental frequency) in Section IV. This estimator is, therefore, especially designed for detecting the emerging problem of oscillations between parallel-connected PV inverters with *LCL* filters.

Consider a power electrical signal comprising a fundamental signal $y_1(t)$ of nominal frequency ω_1, plus other high-frequency components and a dc offset (A_0) as

$$\begin{aligned} y(t) &= A_0 + y_1(t) + \sum_{k=2}^{n} y_k(t) \\ &= A_0 + A_1 \sin(\omega_1 + \phi_1) + \sum_{k=2}^{n} A_k \sin(\omega_k + \phi_k) \end{aligned} \quad (1)$$

where A_k, ω_k, and ϕ_k are the amplitude, frequency, and initial phase of $y_k(t)$, respectively. The amplitudes verify the inequality $A_k \geq 0$, $k = 0, 1, \ldots$; the frequency parameters are strictly positive and unique: $\omega_k > 0$, $\omega_k \neq \omega_j$ for $k \neq j$; and ϕ_k is the unknown initial phase of each sinusoid. Note that the fundamental component is isolated in (1) due to its importance in the context of power system signals. Note that the kth component y_k usually represents the kth-order harmonic, characterized by the harmonic frequency

$$\omega_k = k\omega_1. \quad (2)$$

In case only harmonics are present, the frequencies of the harmonic components need not to be independently estimated and can be derived from (2) by using the estimate of the fundamental frequency. However, the presence of interharmonics is inevitable in practical applications [i.e., ω_k may vary within a neighborhood of $k\omega_1$], thus motivating us to propose this algorithm that can estimate frequencies of all components independently. In view of (1), each sinusoidal component y_k verifies the second-order differential equation $\ddot{y}_k(t) = -\omega_k^2 y_k(t)$.

In the Laplace domain

$$s^2 y_k(s) - s y_k(0) - \dot{y}_k(0) = -\omega_k^2 y_k(s) \quad (3)$$

where s is Laplace variable. By rearranging (3)

$$y_k(s) = \frac{s y_k(0) + \dot{y}_k(0)}{s^2 + \omega_k^2}.$$

Hence, the signal $y(t)$ in the s-domain is expressed as

$$y(s) = \sum_{k=1}^{n} \frac{s y_k(0) + \dot{y}_k(0)}{s^2 + \omega_k^2} + \frac{A_0}{s}$$

which has a characteristic polynomial denoted by $P(s)$ with purely imaginary roots occurring in the a complex-conjugate pair at each frequency

$$\begin{aligned} P(s) &= s \prod_{k=1}^{n} \left(s^2 + \omega_k^2\right) \\ &= s^{2n+1} + a_{n-1} s^{2n-1} + \cdots + a_1 s^3 + a_0 s. \end{aligned} \quad (4)$$

It is worth noting that the frequencies ω_k act as the zeros of $P(s)$. Based on (4), the incoming signal $y(t)$ defined in (1) can be thought as generated by the following autonomous system the eigenvalue of which is identical to the zeros of the characteristic polynomial $P(s)$ [34]:

$$\begin{cases} \dot{x}(t) = A_x x(t) \\ y(t) = c_x^T x(t) + A_0 \end{cases} \quad (5)$$

where

$$\mathbf{A}_x = \begin{bmatrix} 0 & 1 & 0 & \cdots & 0 \\ -a_{n-1} & 0 & 1 & \cdots & 0 \\ \vdots & \ddots & \ddots & \ddots & \vdots \\ 0 & 0 & \ddots & \ddots & 1 \\ -a_0 & 0 & \cdots & \cdots & 0 \end{bmatrix}$$

$$c_x^T = \begin{bmatrix} 1\ 0 \cdots 0\ 0 \end{bmatrix}.$$

In the following discussion, an algorithm that can estimate system's parameters $a_i,\ i = 0,\ 1, 2,\ \ldots$, in a very fast manner is proposed. The frequencies ω_k can be determined from a_i through the relationship implied in (4) (i.e., the roots of the equation $P(j\omega) = 0$).

Comparing to the available methods that mainly deal with the fundamental and harmonic frequencies, the proposed multifrequency strategy offers the flexibility of being able to address more than one sinusoid. This important feature offers a solution to fast online interharmonic detection. As clearly shown in (5), the order of the signal generator model depends on the number of frequencies to be estimated. The residual sinusoidal components (that are not taken into account) are implicitly treated as a disturbance which may result in a degradation of accuracy. However, higher computing load is required by increased dynamic order. In this connection, the computation burden and the precision need to be compromised. Without loss of generality, a generic framework that copes with n harmonics and a possible offset [see (1)] is dealt with in Section III.

III. Frequency Tracking Method Based on Integral Operators

A. Preliminaries

In this section, an estimation scheme is designed for estimating n arbitrary frequencies in a harmonic signal. The fundamental theory behind this method is based on rather complex mathematics, but the suitably designed algorithm can be simply implemented via linear state-space equations. Next, we introduce some basic theories that contribute the further analysis, while the detailed derivation is reported in the appendix.

In this paper, we resort to a typical linear integral operator (see [22] and [35] for more details), defined as

$$[V_K u](t) \triangleq \int_0^t K(t,\tau)\, u(\tau)\, d\tau, \qquad t \in \mathbb{R}_{\geq 0} \quad (6)$$

where $u(t)$ is the processed signal and the function $K(t,\tau)$ is a specialized bivariate kernel function with the form

$$K(t,\tau) \triangleq e^{-\rho(t-\tau)} \left(1 - e^{-\rho\tau}\right)^{2n+1} \left[1 - e^{-\rho(t-\tau)}\right]^{2n+1} \quad (7)$$

where $\rho > 0$ is a design parameter. In the rest of this paper, we denote the ith-order signal derivative as $u^{(i)},\ \ i = 0, 1, 2, \ldots$, for the sake of simplifying the notation. Moreover, given that a kernel function $K(t,\tau)$ has two variables, the ith-order derivative of K with respect to the second argument will be denoted as $K^{(i)}$. The reason for selecting the kernel function is that the integral operator of the derivative $u^{(i)}(t)$ through the specialized kernel $K(t,\tau)$ can be computed by using the image of the available signal $u(t)$ (proof is provided in Appendix A), that is

$$\left[V_K u^{(i)}\right](t) = (-1)^i \left[V_{K^{(i)}} u\right](t).$$

It is worth noting that the ith derivative of the kernel (7) with respect to the second argument can be expressed as

$$K^{(i)}(t,\tau) = \sum_{j=1}^{2n+2} e^{-\rho j t} f_{i,j}(\tau) \quad (8)$$

where $f_{i,j}(\cdot)$ are univariate functions of τ. Let $K_{i,j}(t,\tau) \triangleq (-1)^i e^{-\rho j t} f_{i,j}(\tau)$; then by linearity of the integral operator, it follows that

$$\left[V_K u^{(i)}\right](t) = (-1)^i \left[V_{K^{(i)}} u\right](t) = \sum_{j=1}^{N+1} \left[V_{K_{i,j}} u\right](t).$$

Next, we apply the aforementioned results to devise the fast estimation scheme.

B. Frequency Tracking Strategy

Now let us introduce the differential constraint model of (5) as

$$y^{(2n)}(t) = \sum_{i=0}^{n-1} a_k y^{(2i)}(t) - a_0 A_0\ . \quad (9)$$

By taking the first-order time-derivative on both sides of the structural constraint (9), we obtain

$$y^{(2n+1)}(t) = \sum_{i=0}^{n-1} a_i y^{(2i+1)}(t). \tag{10}$$

Then, we apply the integral operator (6) on both sides of (10), getting to

$$\left[V_{K_{2n+1}} y^{(2n+1)}\right](t) = \sum_{i=0}^{n-1} a_i \left[V_{K_{2n+1}} y^{(2i+1)}\right](t). \tag{11}$$

For the sake of brevity, let $r_i(t) = [V_{K_{2n+1}} y^{(i)}](t)$, $i = 0, 1, \ldots 2n+1$, (11) can be rewritten as

$$r_{2n+1}(t) = \sum_{i=0}^{n-1} a_i r_{2i+1}(t). \tag{12}$$

By introducing the true parameter vector

$$\theta^* \triangleq \left[\, a_0 \; a_1 \; \cdots \; a_{n-2} \; a_{n-1} \,\right]^T$$

and the vector of auxiliary signals that collect only the odd derivative indices

$$z(t) \triangleq \left[\, r_1(t), r_3(t) \quad \cdots \; r_{2n-1}(t) \,\right]^T.$$

Equation (12) can be rewritten in compact form as

$$z^T(t)\,\theta^* = r_{2n+1}(t). \tag{13}$$

The modulated signal $r_i(t)$, $i = 0, 1, \ldots, 2n+1$, can be obtained as the output of an $(2n+2)$th dimensional linear time-varying dynamical system, described as (the derivation is given in Appendix B)

$$\begin{cases} \xi_i^{(1)}(t) = \boldsymbol{G}\xi_i(t) + \boldsymbol{E}_i(t)\, y(t) \\ r_i(t) = \boldsymbol{H}\xi_i(t) \end{cases} \tag{14}$$

with $\xi_i(0) = 0$ and where the other quantities in (14) are

$$\begin{aligned} \mathbf{G} &= \operatorname{diag}\left(-\rho, -2\rho, \ldots, -\rho\,(2n+2)\right) \\ \mathbf{E}_i(t) &= \begin{bmatrix} K_{i,1}(t,t) \\ \vdots \\ K_{i,2n+2}(t,t) \end{bmatrix} \\ H &= [1, 1. \ldots, 1]. \end{aligned} \tag{15}$$

By employing $n+1$ systems of the kind (14) comprising the set of $\mathbf{E}_i(t)\ \forall 1, 3, \ldots, 2n+1$, both the vectors of signals $z(t)$ and r_{2n+1} [that are needed to form the constraint (13)] can be determined.

Note that (13) represents a standard linear expression for identification. Conventional augmentation tools used in system identification can be employed to form a well-posed algebraic system based on (13). Let us first multiply both sides of (13) by $z(t)$

$$R(t)\,\theta^* = S(t) \tag{16}$$

where $R(t)$ and $S(t)$ are the so-called auto-covariance and cross-covariance matrices defined as

$$R(t) \triangleq z(t)\, z^T(t), \qquad S(t) \triangleq z(t)\, r_{2n+1}(t).$$

In order to avoid singularity of the instantaneous auto-covariance matrix $R(t)$ (i.e., rank 1 at any time instant). We apply to both sides of (16) a simple second-order low-pass filter that is described by transfer function representation

$$F(s) = \frac{w_c^2}{s^2 + \lambda w_c s + w_c^2} \tag{17}$$

for faster frequency response than the first order, while maintaining a low level of complexity.

Therefore, the following relationship holds for all $t \geq 0$:

$$\mathcal{L}^{-1}\left\{F(s)\,R(s)\right\}(t)\,\theta^* = \mathcal{L}^{-1}\left\{F(s)\,S(s)\right\}(t) \tag{18}$$

where $\mathcal{L}^{-1}$ denotes the operation of the inverse Laplace transform. Defining $R_f(t) = \mathcal{L}^{-1}\{F(s)R(s)\}(t)$ and $S_f(t) = \mathcal{L}^{-1}\{F(s)S(s)\}(t)$, an estimate $\hat{\theta}(t)$ of the parameter vector θ^* can be obtained by minimizing the quadratic criterion

$$\hat{\theta}(t) = \arg\min_{\theta^*} \left\| R_f(t)\theta^* - S_f(t) \right\|.$$

In this case, the unknown parameter vector θ^* can be estimated by

$$\hat{\theta}(t) = \begin{cases} \theta_0, & t < t_\epsilon \\ R_f(t)^{-1} S_f(t), & t \geq t_\epsilon \end{cases} \tag{19}$$

where θ_0 is a guessed parameter vector depending on the nominal frequency values, and $t_\epsilon > 0$ is a small time constant, needed because $R_f(t)$ is not invertible at $t = 0$ (i.e., $R_f(0) = 0$). Finally, as mentioned before, the frequencies $\omega_1, \ldots, \omega_n$ are computed by letting

$$P(j\omega) = 0 \tag{20}$$

where $P(j\omega)$ is parametrized by a_i as given in (4).

A structural block diagram of the proposed algorithm is shown in Fig. 1, where the $n+1$ identical system [see (14)] is enhanced by dotted rectangles and $y(t)$ is the incoming signal.

Remark 1: Note that the algebra algorithm (19) is valid only when the filtered auto-covariance matrix $R_f(t)$ is invertible. The invertibility of $R_f(t)$ characterizes a sufficiently informative output signal at time t. In view of (14), the parameter ρ determines the poles of $\mathbf{G}$ that in turn determines the cutoff frequency of the overall low-pass filtering structure. A larger ρ results in a poorer noise immunity, while a smaller ρ may result in a less informative $R_f(t)$ due to the excessive attenuation of $y(t)$. To this end, the choice of ρ depends on *a priori* information of the frequency band of the interharmonic.

Remark 2: The low-pass filter (17) is applied on both sides of (18), then the parameter vector $\hat{\theta}(t)$ is determined algebraically by $R_f(t)^{-1} S_f(t)$, by which the estimation results are independent of the low-pass filter. However, to avoid excessive attenuation that may lead to numerical issue, the rules given in Remark 1 also apply to the design of filtering parameter λ and w_c.

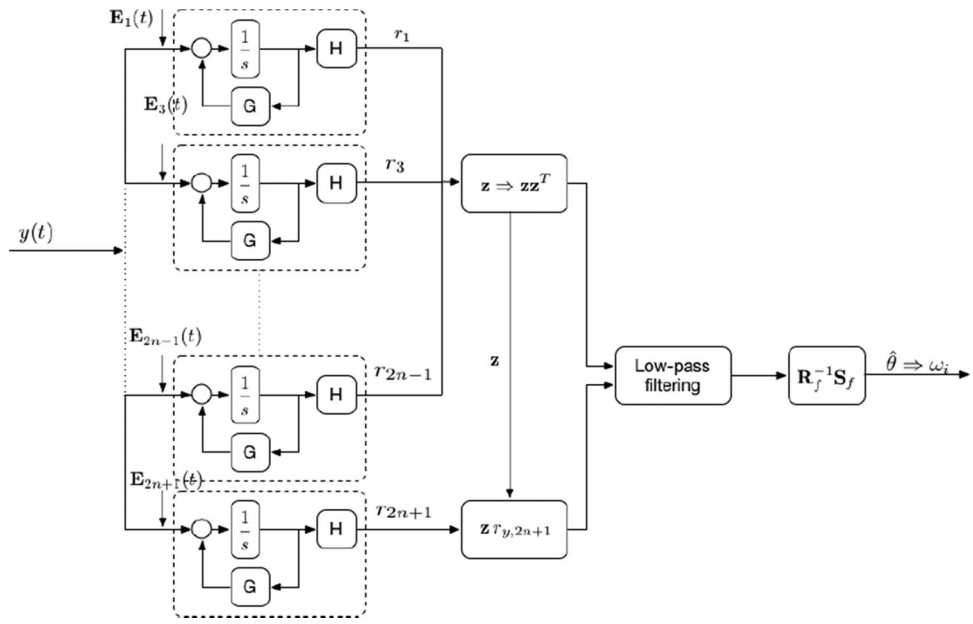

Fig. 1. Block diagram of the proposed algorithm.

IV. Adoption of the Algorithm for Tracking Fundamental and Interharmonic Components

In this section, the proposed estimator is adopted for detecting and tracking the fundamental and a typical interharmonics. For practical applications of grid-connected power inverters, the fundamental frequency is selected as 50 Hz and the interharmonic frequency as 1.94 kHz (representing the occurrence of resonance between parallel grid-connected power inverters). Note that the use of the integral observer algorithm for detecting total harmonics has been reported in [23] and is, thus, not repeated here. The mains voltage signal can be expressed as

$$v\left(t\right) = v_1\left(t\right) + v_m\left(t\right) + \sum_{k=2}^{n\backslash m} v_k\left(t\right) \tag{21}$$

where t is the time variable, $v_1(t)$ is the fundamental voltage, $v_m(t)$ is the interharmonic that needs to be identified, and $\sum_{k=2}^{n\backslash m} v_k(t)$ is the total harmonic voltage apart from $v_m(\mathrm{t})$. For the sake of further analysis, let us consider

$$y\left(t\right) = v_1\left(t\right) + v_m\left(t\right).$$

It is important to note that the estimator considers the remaining harmonics $\sum_{k=2}^{n\backslash m} v_k(t)$ as "noise" initially. The schematic of this method is shown in Fig. 2. It should be noted that the band-stop filter is employed to attenuate the impact of the "noise" term (harmonics and pure noise) since the magnitude of the interharmonic is very small. The band-stop filter is an elliptic type with 80 Hz and 1800 Hz, respectively, for the lower and upper passband edge. Although the elliptic filter suffers from passband and stopband ripples, it is chosen for its fast frequency response, which is an important attribute for this application.

Now, $y(t)$ can be thought as generated by the following autonomous system:

$$\begin{cases} \dot{x}\left(t\right) = A_x x\left(t\right) \\ y\left(t\right) = c_x^T x\left(t\right) \end{cases} \tag{22}$$

where

$$\mathbf{A}_x = \begin{bmatrix} 0 & 1 & 0 & 0 \\ a_1 & 0 & 1 & 0 \\ 0 & 0 & 0 & 1 \\ a_0 & 0 & 0 & 0 \end{bmatrix}$$

$$c_x^T = \begin{bmatrix} 1\,0 & 0\,0 \end{bmatrix}.$$

The state-space system (22) leads to the next differential constraint model

$$y^{(4)}\left(t\right) = a_1 y^{(2)}\left(t\right) + a_0 y\left(t\right). \tag{23}$$

Applying the linear integral operator to both side of (23) with a kernel function in the form of (6) with the order of the multiplier reduced from $2n+1$ to 4 and ρ is designed as 1000

$$K\left(t,\tau\right) \triangleq e^{-1000(t-\tau)}\left(1-e^{-1000\tau}\right)^4\left[1-e^{-1000(t-\tau)}\right]^4$$

we obtain

$$r_4\left(t\right) = \begin{bmatrix} r_0\left(t\right) & r_2\left(t\right) \end{bmatrix}\begin{bmatrix} a_0 \\ a_1 \end{bmatrix} = z^T\left(t\right)\theta^* \tag{24}$$

where $r_i(t) = [V_K y^{(i)}](t),\ \ i = 0,\ 2,\ 4.$

Moreover, $r_i(t),\ \ i = 0,\ 2,\ 4$, can be respectively obtained as the output of a fifth-order linear time-varying dynamical system, described as

$$\begin{cases} \xi_i^{(1)}\left(t\right) = \boldsymbol{G}\xi_i\left(t\right) + \boldsymbol{E}_i\left(t\right) y\left(t\right) \\ r_i\left(t\right) = \boldsymbol{H}\xi_i\left(t\right) \end{cases}$$

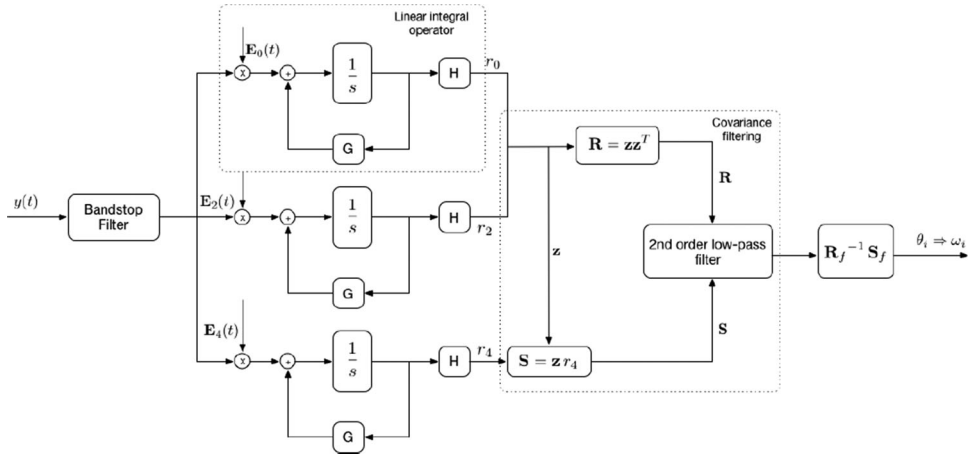

Fig. 2. Schematic of the estimation algorithm.

with $\xi_i(0)=0$ and

$$\mathbf{G}=\operatorname{diag}\left(-1000,-2000,-3000,-4000,\ -5000\right)$$

$$\mathbf{E}_i\left(t\right)=\begin{bmatrix}K_{i,1}\left(t,t\right)\\K_{i,2}\left(t,t\right)\\K_{i,3}\left(t,t\right)\\K_{i,4}\left(t,t\right)\\K_{i,5}\left(t,t\right)\end{bmatrix}$$

$$H=\begin{bmatrix}1 & 1 & 1 & 1 & 1\end{bmatrix}. \tag{25}$$

Note that the elements of $\mathbf{E}_i(t),\ \ i=0,\ 2,\ 4$ can be determined based on (8) by symbolic computation tools. The expressions are given as follows: this unnumbered equation shown at the bottom of this page.

Finally, (24) can be solved by following the same steps shown in the generic case.

Step 1: Multiplying both sides of (24) by $z(t)$ leads to

$$R\left(t\right)\theta^{*}=S\left(t\right) \tag{26}$$

with

$$R\left(t\right)\triangleq z\left(t\right)z^{T}\left(t\right),\qquad S\left(t\right)\triangleq z\left(t\right)r_4\left(t\right).$$

Step 2: Apply to both sides of (26) a low-pass filter in the form of (17), with $\lambda=4,\ w_c=350$

$$F\left(s\right)=\frac{w_c^2}{s^2+\lambda w_c s+w_c^2}$$

such that

$$R_f\left(t\right)\theta^{*}=S_f\left(t\right)\left(t\right) \tag{27}$$

where $R_f(t)=\mathcal{L}^{-1}\{F(s)R(s)\}(t)$ and $S_f(t)=\mathcal{L}^{-1}\{F(s)S(s)\}(t)$.

$$\mathbf{E}_0\left(t\right)=\begin{bmatrix}K_{0,1}\left(t,t\right)\\K_{0,2}\left(t,t\right)\\K_{0,3}\left(t,t\right)\\K_{0,4}\left(t,t\right)\\K_{0,5}\left(t,t\right)\end{bmatrix}=\begin{bmatrix}-1000\left(3e^{-1000t}+1\right)\left(e^{-1000t}-1\right)^3\\8000\left(e^{-1000t}+1\right)\left(e^{-1000t}-1\right)^3\\-6000\left(e^{-1000t}+3\right)\left(e^{-1000t}-1\right)^3\\16000\left(e^{-1000t}-1\right)^3\\1000\left(e^{-1000t}-5\right)\left(e^{-1000t}-1\right)^3\end{bmatrix}$$

$$\mathbf{E}_2\left(t\right)=\begin{bmatrix}K_{2,1}\left(t,t\right)\\K_{2,2}\left(t,t\right)\\K_{2,3}\left(t,t\right)\\K_{2,4}\left(t,t\right)\\K_{2,5}\left(t,t\right)\end{bmatrix}=\begin{bmatrix}-1000^3\left(27e^{-4000t}-32e^{-3000t}+6e^{-2000t}-1\right)\\16\times1000^3\left(2e^{-4000t}-e^{-3000t}+e^{-1000t}-2\right)\\-6\times1000^3\left(e^{-4000t}-6e^{-2000t}+32e^{-1000t}-27\right)\\16\times1000^3\left(e^{-3000t}-12e^{-2000t}+27e^{-1000t}-16\right)\\1000^3\left(e^{-4000t}-32e^{-3000t}+162e^{-2000t}-256e^{-1000t}+125\right)\end{bmatrix}$$

$$\mathbf{E}_4\left(t\right)=\begin{bmatrix}K_{4,1}\left(t,t\right)\\K_{4,2}\left(t,t\right)\\K_{4,3}\left(t,t\right)\\K_{4,4}\left(t,t\right)\\K_{4,5}\left(t,t\right)\end{bmatrix}=\begin{bmatrix}-1000^5\left(243e^{-4000t}-128e^{-3000t}+6e^{-2000t}-1\right)\\16\times1000^5\left(8e^{-4000t}-e^{-3000t}+e^{-1000t}-8\right)\\-6\times1000^5\left(e^{-4000t}-6e^{-2000t}+128e^{-1000t}-243\right)\\16\times1000^5\left(e^{-3000t}-48e^{-2000t}+243e^{-1000t}-256\right)\\1000^5\left(e^{-4000t}-128e^{-3000t}+145e^{-2000t}-4096e^{-1000t}+3125\right)\end{bmatrix}.$$

Step 3: The estimate $\hat{\theta}(t) = [a_0 \quad a_1]^T$ of the unknown parameter vector θ^* is obtained by

$$\hat{\theta}(t) = \begin{cases} \theta_0, & t < t_\epsilon \\ R_f(t)^{-1} S_f(t), & t \geq t_\epsilon \end{cases} \tag{28}$$

where θ_0 is a guessed parameter vector depending on the nominal frequency values, and $t_\epsilon > 0$ is a small time constant. $t_\epsilon > 0$ is needed because $R_f(t)$ is not invertible at $t = 0$ (i.e., $R_f(0) = 0$).

Step 4: The frequencies ω_1 and ω_m of the fundamental and the interharmonic are indirectly estimated as the roots of the following equation:

$$s^4 - a_1 s^2 - a_0 = 0. \tag{29}$$

The coefficients of a_0 and a_1 have to be dynamically determined through Steps 1–3. If only the fundamental component exists, (29) provides only one unique real solution. If both of the fundamental and interharmonics are present, it gives two unique solutions.

For fast detection of the interharmonic, the matrix $R_f(t)$ is utilized in addition to the frequency estimates. Let us consider $\sigma_{\min}(R_f(t))$ as the minimum eigenvalue of $R_f(t)$. According to the concept of persistency of excitation, $\sigma_{\min}(R_f(t))$ can be used as an indicator to capture the existence of the interharmonic [25]. More specifically, when the algorithm is fed by a combination of fundamental and interharmonic, $\sigma_{\min}(R_f(t))$ is inherently sinusoidal with the mean above a certain level depending on the amplitude of the input in the steady state. As soon as the interharmonic vanishes, $\sigma_{\min}(R_f(t))$ quickly decays and moves back only when the interharmonic appears again. In this connection, we proposed a mechanism for estimating interharmonic with a properly designed threshold. The frequency estimate of the interharmonic is driven to 0 (an indication of no interharmonic) as soon as $\sigma_{\min}(R_f(t))$ falls below the threshold. On the other hand, the initial condition of the frequency estimates is reset by a value within the possible range of interharmonic frequency when the indicator reach the threshold again, thus significantly saving the time for convergence.

V. Experimental Verification

In order to evaluate the effectiveness of the proposal method in detecting the fundamental and interharmonic, a programmable power supply is used to generate the required voltage waveforms. Because the proposed algorithm provides numerical values of the frequency components, digital-to-analog (D/A) converters are used to generate analogue signals that represent the fundamental and interharmonics components. The fundamental frequency is 50 Hz, while the targeted interharmonic is within the targeted frequency band of 1.7–2.0 kHz (using the examples of [11] and [12]). The algorithm is implemented in a dSpace DS1006 system with a CPU clock rate of 2.8 GHz and a memory size of 1 GB (SDRAM) (see Fig. 3). The sampling frequency of the dSpace system is 10 kHz. Because of the widely separated fundamental frequency and the interharmonic, their frequency values are scaled with the frequency-to-voltage ratios of 1:10 and 1:25, respectively, so that the frequency values can be displayed as voltage signals in a digital storage oscilloscope in real time. In this section, the fundamental frequency, the interharmonic frequency, and the input signal are in the measured waveforms in the figures as the green, blue, and yellow traces, respectively.

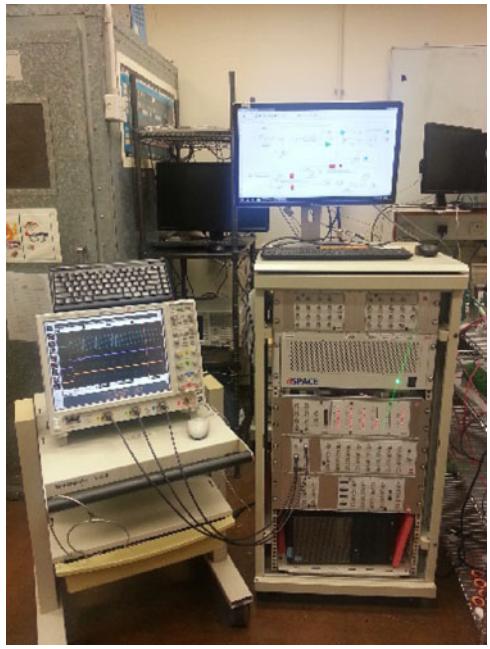

Fig. 3. Photograph of the experimental setup with the dSpace system and digital oscilloscope.

A. Steady-State Estimation

The first test is to generate a fundamental signal at 50 Hz with a superimposed high-frequency signal at 1.94 kHz (i.e., representing the interharmonic). This signal is sampled by the dSpace A/D system, and digitized for use in the proposed algorithm. The sampling rate of the dSpace system is 10 kHz, meaning that the adopted algorithm can be executed within 100 μs. The computational time of the algorithm in the dSpace system is about 55 μs. The actual and computed fundamental frequency and interharmonic frequency are displayed in Fig. 4 and tabulated in Table I. These results show that the practical and computed frequencies are in good agreement. Adding extra frequency detection functions will inevitably increase the computational burden of the microcontroller of the power inverter. If such computational needs exceed the computational capabilities (e.g., speed) of the microcontroller, additional processor may be needed to implement the frequency detection functions.

B. Sudden Appearance of Interharmonic

The second test emulates the sudden occurrence of the resonance of the *LCL* filters between parallel PV systems. The power source is programmed initially with the fundamental component of 50 Hz only. Then, the interharmonic component is added to the fundamental component. The measured input voltage signal provided by the power source is shown with the analog version of the fundamental frequency and interharmonic frequency in

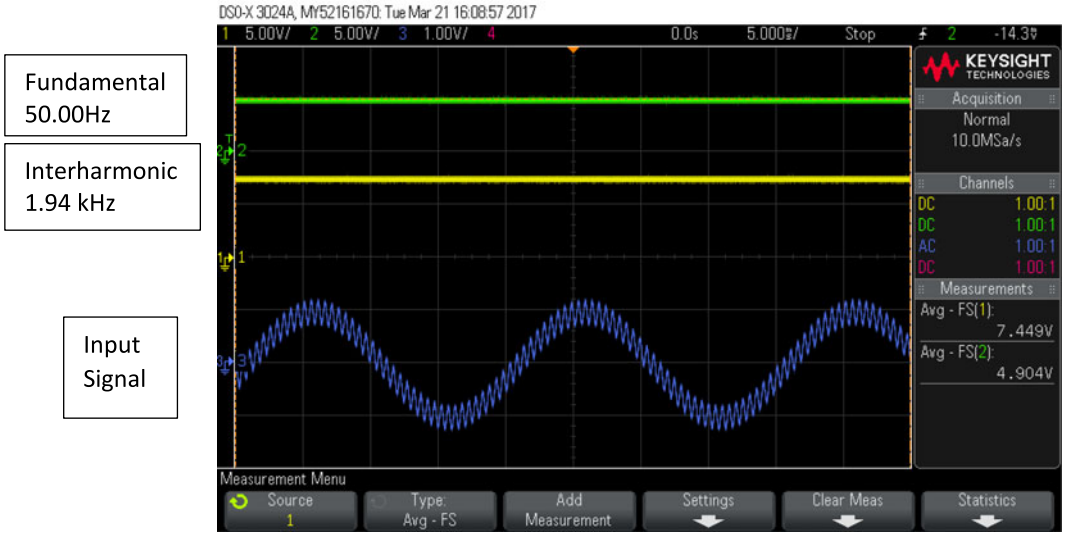

Fig. 4. Practical input signal with fundamental frequency of 50 Hz superimposed with an interharmonic of 1.94 kHz, and the analog versions of the computed fundamental and interharmonic frequency (5 ms/div)

TABLE I
INFORMATION OF FUNDAMENTAL AND INTERHARMONIC FREQUENCY

	Fundamental frequency	Interharmonic frequency
Actually programmed in power source	50.000	1.94 kHz
Computed by proposed method	50.007	1.99 kHz

Fig. 5. The time scale is set at 5 ms/div. It can be observed that the fundamental frequency remains constant through the test because its analog version remains a straight horizontal line during the step change of the interharmonic.

The kernel signal is used to provide fast detection of the interharmonic. It is the eigenvalue of the matrix signal $R_f(t)$ that is composed of processed versions (filtered) of the incoming signal $y(t)$. So the kernel signal is an inherent sinewave because of the sinusoidal nature of $y(t)$. When the inharmonic is absent, the kernel signal is zero. When the interharmonic appears, the kernel signal increases from zero. Therefore, when the kernel signal increases beyond a threshold ΔV_1, it can trigger the signal of interharmonic occurrence from 0 to 1. The kernel signal will then rise until it settles down to a steady-state level (with a sinusoidal ac ripple). A moving window method is used to locate the minimum kernel value for each period of the kernel signal (i.e., half period of the mains voltage). When the interharmonic disappears, the kernel signal will decay to zero. Thus, when the kernel signal is less than the minimum kernel value by another threshold ΔV_2, it can trigger the signal of the interharmonic occurrence from 1 to 0. As long as the thresholds ΔV_1 and ΔV_2 are slightly larger than the noise level, the detection times can be minimized. In the practical tests, ΔV_1 and ΔV_2 are set at 0.098 V and 0.188 V, respectively.

It is, however, important to note that the harmonic detection time from 0 to 1 is usually very fast because the initial kernel signal is zero and has no ripple. This feature is important and advantageous because the purpose of the algorithm is to detect the occurrence of the interharmonic in this specific application as the signal for the occurrence of resonance between parallel grid-connected power inverters. In Fig. 5, the detection time for the occurrence of the interharmonic is only 3 ms. This detection time can be reduced if ΔV_1 is further reduced, as long as ΔV_1 is larger than the noise level in the practical implementation.

C. Sudden Disappearance of Interharmonic

The third test focuses on the sudden disappearance of the interharmonic. This is to emulate the situation that the resonance between the parallel *LCL* filters has stopped. The corresponding measured signals are displayed in Fig. 6. Fig. 5 shows that the kernel signal will reach its steady waveform within about one mains cycle. Such waveform is used again for detecting the disappearance of the interharmonic. When the kernel value falls to a value less than the minimum value by a certain threshold, it signifies the absence of the interharmonic. In this case, it takes about 9 ms to detect the disappearance of the interharmonic. This detection time is less than half of a mains cycle. In Fig. 6, the kernel signal at the high state has some ripple. The trigger signal has to wait for the kernel signal to drop below the minimum kernel signal in the moving window by ΔV_2 before changing from one to zero. This is why the detection time for the disappearance of the interharmonic is longer than that for the occurrence of the interharmonic.

D. Variation of Mains Frequency

The fourth test considers the possibility of mains frequency variation due to the increasing use of intermittent renewable energy penetration in power grid, especially microgrid using small electric generators. Normally, large-scale power grids do not have rate of change of frequency (RoCoF) higher than 0.1 Hz/s. For U.K., the RoCoF is limited at 0.2 Hz/s [24]. For micro-

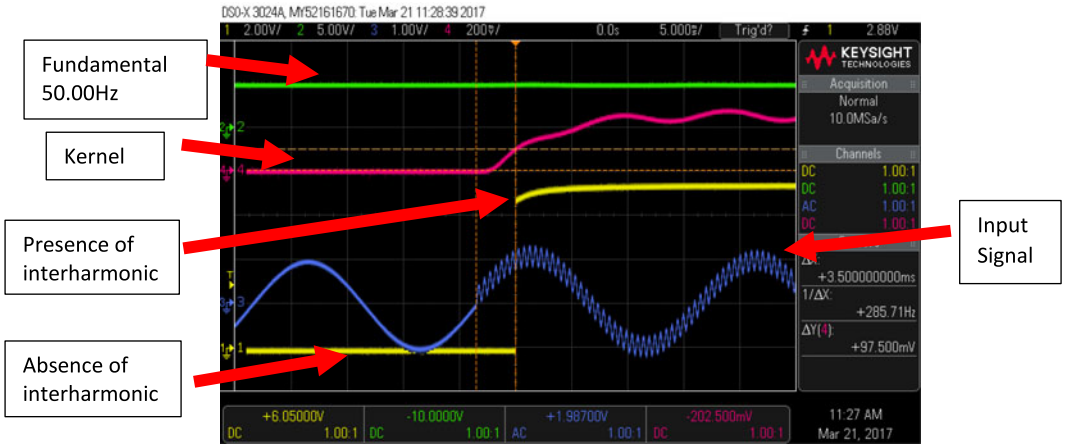

Fig. 5. Practical input signal with fundamental frequency of 50 Hz superimposed with an interharmonic of 1.94 kHz, and the analog versions of the computed fundamental and interharmonic frequency (5 ms/div).

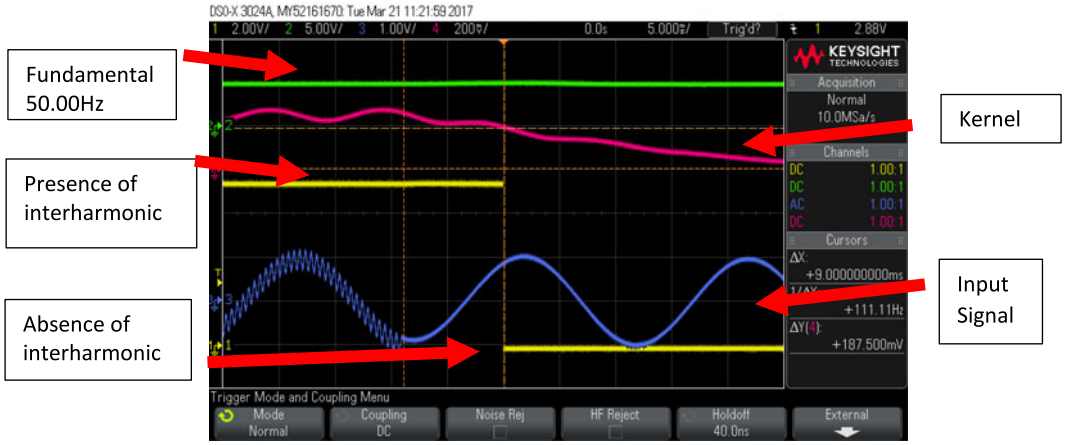

Fig. 6. Practical input signal with fundamental frequency of 50 Hz superimposed with an interharmonic of 1.94 kHz, and the analog versions of the computed fundamental and interharmonic frequency (5 ms/div).

grid, a higher RoCoF of 0.5 Hz/s is adopted in this test. The RoCoF is programmed in a linear manner so that the frequency value ramps up and down between 48 and 52 Hz. For a RoCoF of 0.5 Hz/s, the mains frequency changes from 48 to 52 Hz in 8 s.

Fig. 7 shows the input signal comprising the fundamental frequency superimposed with an interharmonic of 1.94 kHz, with the fundamental frequency varying between 48 and 52 Hz. It can be seen that the analog version of the fundamental frequency varies within 48 and 52 Hz linearly as expected, while the analog version of the interharmonic frequency remains constant. These results indicate that even if the mains frequency varies, the successful detection of interharmonic remains intact.

E. Further Discussion

For the targeted interharmonic frequency range of 1.7 to 2 kHz, the choice of 1.94 kHz in Section V-D represents the upper end of the range. The proposed method has been tested with an interharmonic of 1.64 kHz, which is at the lower end of the range. The fundamental frequency remains at 50 Hz. Fig. 8 shows the measurements when a smaller threshold (ΔV_1) is adopted. Note that the time scale of Fig. 8 is 2 ms/div (instead of 5 ms/div as in Figs. 3–5). With a lower threshold, the detection time is reduced to about 1.5 ms. Therefore, for the typical interharmonic frequency range of 1.7–2 kHz reported in [11] and [12], the proposed method can detect the occurrence of interharmonic within a few milliseconds. In principle, the proposed method can detect multiple frequencies. The demonstration in this paper is specific to potential applications such as resonance between parallel grid-connected power inverters.

One possible application of the proposed algorithm is to detect the interharmonic arising from parallel operations of grid-connected inverters with *LCL* filters. Fig. 9 shows a typical setup based on the *LCL* filter parameters previously reported in [8]. The inverters are operated at a switching frequency of 3.78 kHz. A real-time simulation on this setup is used to demonstrate the interharmonic oscillation between the power inverters. The total current injected into the grid is captured and outputted as a real-time signal for analysis with the proposed algorithm. Fig. 10

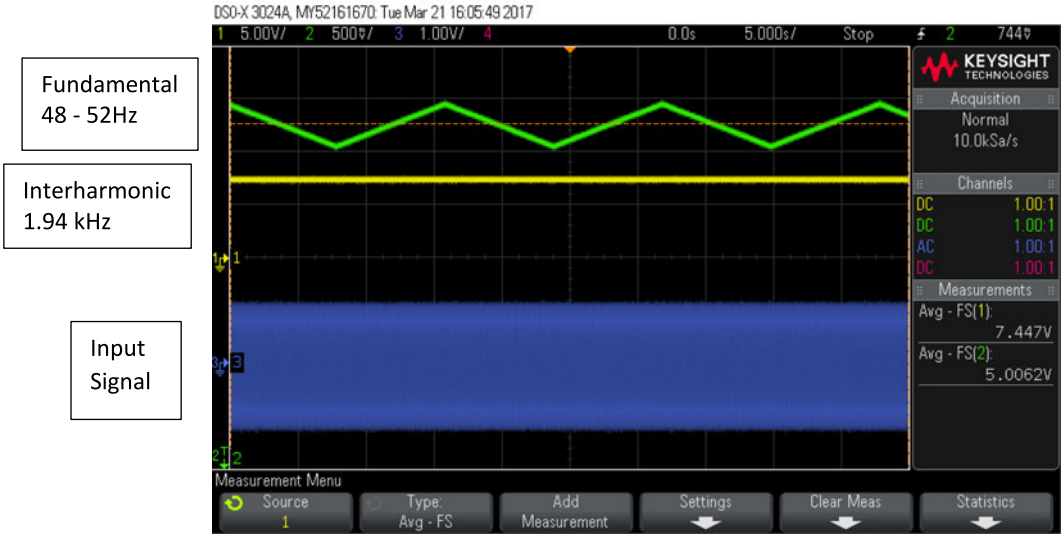

Fig. 7. Practical input signal with fundamental frequency (48–52 Hz) superimposed with an interharmonic of 1.94 kHz, and the analog versions of the computed fundamental and interharmonic frequency (5 s/div).

Fig. 8. Practical input signal with fundamental frequency of 50 Hz superimposed with an interharmonic of 1.64 kHz, and the analog versions of the computed fundamental and interharmonic frequency (2 ms/div).

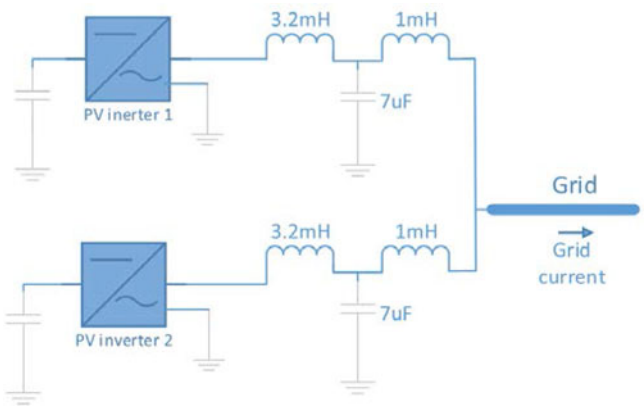

Fig. 9. Schematic of a case study based on two parallel grid-connected inverters.

shows the injected current waveform and the signals representing the fundamental component and interharmonic component (captured immediately when the test begins). The computed fundamental frequency is 49.66 Hz and the interharmonic frequency is 1.387 kHz.

The original algorithm [22] was designed to detect n unknown frequencies. Previously, it has been used to detect harmonics for active power filter applications. In this project, we demonstrate its use for the detection of the fundamental and interharmonics. Since the frequency estimates tend to converge to the frequencies with greater amplitude, the introduction of a band-pass filter is needed to identify the interharmonic (which typically has a much smaller amplitude than the fundamental frequency). But the cutoff frequency of the band-pass filter is hardly dependent on the interharmonic. In this application, it is simply set at a value higher than the fundamental frequency. If the

Fig. 10. Current injected into the grid and the signals of the fundamental and interharmonic components (5 V/div for the three traces; 50 ms/div).

information of the interharmonic is unknown, a higher order estimation scheme of the general algorithm (that takes more frequencies into consideration) has to be adopted.

VI. Conclusion

This paper presents the first practical implementation of an observer-based algorithm for fast detection of fundamental signal and interharmonic component. The theory behind the algorithm has been summarized and explained. The algorithm is adopted in a form for monitoring the presence of the mains frequency and the interharmonic and for estimating their values. A novel method of using the kernel signal for fast interharmonic detection has been proposed and practically demonstrated. Experimental results have confirmed that the detection times of the fundamental and interharmonic can be achieved within half of a mains cycle. This method is suitable for applications such as monitoring the occurrence of resonance between parallel *LCL* filters of grid-connected inverters.

Appendix A

Assuming that the signal $u(t)$ admits the ith-order derivative for $t \geq 0$ and a kernel $K(t,\tau)$ that admits the ith-order derivative with respect to the second argument, the following relationship holds (obtained by means of the integration by parts [35]):

$$\left[V_K u^{(i)}\right](t) = \sum_{j=0}^{i-1} (-1)^{i-j-1} u^{(j)}(t) K^{(1-j-1)}(t,t) + \sum_{j=0}^{i=1} (-1)^{i-1} u^{(j)}(0) K^{(i-j-1)}(t,0) + (-1)^i [V_{K^{(i)}} u](t).$$

It implies that $[V_K u^{(i)}](\cdot)$ can be obtained by the lower order time-derivatives of the processed signal u, $u^{(1)}, \ldots u^{(i-1)}$, which are usually unavailable in real time. However, if a kernel K verifies the following conditions:

$$K^{(j)}(t,0) = 0, \quad \text{(A1-a)}$$

$$K^{(j)}(t,t) = 0, \quad \text{(A1-b)}$$

for all $t \geq 0$ and $i = 0, 1, \ldots, i-1$, then the linear integral of a derivative signal $u^{(i)}$ can be expressed as

$$\left[V_K u^{(i)}\right](t) = (-1)^i \left[V_{K^{(i)}} u\right](t) \quad \text{(A2)}$$

where the right-hand side only depends on the available kernel function K and the signal $u(t)$ per se, thus evading the unavailability of signal derivatives.

By adopting the following bivariate function proposed in [35]:

$$K(t,\tau) \triangleq e^{-\rho(t-\tau)} \left(1 - e^{-\rho\tau}\right)^N \left[1 - e^{-\rho(t-\tau)}\right]^N \quad \text{(A3)}$$

the condition (A1-a) is met by the factor $(1 - e^{-\rho\tau})^N$ up to Nth order, while the condition (A2-b) is met by the third factor $(1 - e^{-\rho(t-\tau)})^N$.

Appendix B

We now describe how such a transformed signal can be obtained as the output of a linear system. First, Let $\xi(t) = [V_K u](t)$ [defined in (6)], by applying the Leibnitz rule in deriving the integral, the signal $[V_K u](t)$, for $t > 0$, can be obtained as the output of a dynamic system described as follows:

$$\begin{cases} \xi^{(1)}(t) = \int_0^t \left(\frac{\partial}{\partial t} K(t,\tau)\right) u(\tau)\, d\tau + K(t,t)\, u(t) \\ [V_K u](t) = \xi(t) \end{cases} \quad \text{(B1)}$$

where $\xi(t) = \xi^{(1)}(t) = 0$.

Since the *i*th derivative of the kernel (A3) with respect to the second argument can be expressed as

$$K^{(i)}(t,\tau) = \sum_{j=1}^{N+1} e^{-\rho j t} f_{i,j}(\tau) \tag{B2}$$

where $f_{i,j}(\cdot)$ are univariate functions of τ. Let $K_{i,j}(t,\tau) \triangleq (-1)^i e^{-\rho j t} f_{i,j}(\tau)$; then by linearity of the integral operator, it follows that

$$\left[V_K u^{(i)}\right](t) = (-1)^i \left[V_{K^{(i)}} u\right](t) = \sum_{j=1}^{N+1} \left[V_{K_{i,j}} u\right](t).$$

Moreover, letting $\xi_{i,j}(t) \triangleq [V_{K_{i,j}} u](t)$, with $i \in \{0,\dots,n\}$, $j \in \{1,\dots,N+1\}$, and taking into account that for all $t \geq 0$, we have

$$\begin{aligned} K_{N|i,j}(t,0) &= 0 \\ \frac{\partial}{\partial t} K_{N|i,j}(t,\tau) &= -\rho j e^{-\rho j t} f_{N|i,j}(\tau). \end{aligned}$$

Thanks to (B1), $[V_{K_N} u]$ admits the following $(N+1)$th dimensional state-space realization:

$$\begin{cases} \xi_{i,j}^{(1)}(t) = -\rho j \xi_{i,j}(t) + K_{i,j}(t,t)\, u(t) \\ \left[V_K u^{(i)}\right](t) = \sum_{j=1}^{N+1} \xi_{i,j}(t) \end{cases} \tag{B3}$$

with $\xi_{i,j}(0) = 0 \quad \forall j = 1,\dots,N+1$.

REFERENCES

[1] F. Blaabjerg, Z. Chen, and S. B. Kjaer, "Power electronics as efficient interface in dispersed power generation systems," *IEEE Trans. Power Electron.*, vol. 19, no. 5, pp. 1184–1194, Sep. 2004.

[2] E. Twining and D. Holmes, "Grid current regulation of a three-phase voltage source inverter with an LCL input filter," *IEEE Trans. Power Electron.*, vol. 18, no. 3, pp. 888–895, May 2003.

[3] J. H. R. Enslin and P. J. M. Heskes, "Harmonic interaction between a large number of distributed power inverters and the distribution network," *IEEE Trans. Power Electron.*, vol. 19, no. 6, pp. 1586–1593, Nov. 2004.

[4] M. Liserre, R. Teodorescu, and F. Blaabjerg, "Stability of photovoltaic and wind turbine grid-connected inverters for a large set of grid impedance values," *IEEE Trans. Power Electron.*, vol. 21, no. 1, pp. 263–272, Jan. 2006.

[5] R. Juntunen, J. Korhonen, T. Musikka, L. Smirnova, O. Pyrh¨onen, and P. Silventoinen, "Identification of resonances in parallel connected grid Inverters with LC- and LCL-filters," in *Proc. IEEE Appl. Power Electron. Conf. Expo.*, 2015, pp. 2122–2127.

[6] M. Lu, X. Wang, P. C. Loh, and F. Blaabjerg, "An analysis method for harmonic resonance and stability of multi-paralleled LCL-filtered inverters," in *Proc. IEEE 6th Int. Symp. Power Electron. Distrib. Gener. Syst.*, Aachen, Germany, 2015, pp. 1–6.

[7] M. Lu, X. Wang, P. C. Loh, and F. Blaabjerg, "Interaction and aggregated modeling of multiple paralleled inverters with LCL filter," in *Proc. IEEE Energy Convers. Congr. Expo.*, 2015, pp. 1954–1959.

[8] M. Lu, X. Wang, P. C. Loh, and F. Blaabjerb, "Resonance interaction of multiparallel grid-connected inverters with LCL filter," *IEEE Trans. Power Electron.*, vol. 32, no. 2, pp. 894–899, Feb. 2017.

[9] J. He, Y. Li, and D. Bosnjak, "Investigation and active damping of multiple resonances in a parallel-inverter-based microgrid," *IEEE Trans. Power Electron.*, vol. 28, no. 1, pp. 234–246, Jan. 2013.

[10] X. Wang, F. Blaabjerg, M. Liserre, and Z. Chen, "An active damper for stabilizing power-electronics-based AC systems," *IEEE Trans. Power Electron.*, vol. 29, no. 7, pp. 3318–3328, Jul. 2014.

[11] X. Lu, K. Sun, L. Huang, M. Liserre, and F. Blaabjerg, "An active damping method based on biquad digital filter for parallel grid-interfacing inverters with LCL filters," in *Proc. 2014 29th Annu. IEEE Appl. Power Electron. Conf. Expo.*, Mar. 16–20, 2014, pp. 392–397.

[12] H. Wang, P. Zhang, J. Su, and G. Zhang, "Resonant mechanism of multi grid-connected inverters in distribution power systems," in *Proc. IEEE Energy Convers. Congr. Expo.*, 2015, pp. 1729–1735.

[13] T. X. Zhu, "Exact harmonics/interharmonics calculation using adaptive window width," *IEEE Trans. Power Del.*, vol. 22, no. 4, pp. 2279–2288, Oct. 2007.

[14] I. Y.-H. Gu and M. H. J. Bollen, "Estimating interharmonics by using sliding-window ESPRIT," *IEEE Trans. Power Del.*, vol. 23, no. 1, pp. 13–23, Jan. 2008.

[15] M. Caixba and A. Ramirez, "Enhanced switching function matrix calculation in the interharmonic domain," in *Proc. IEEE PES Gen. Meeting*, 2010, pp. 1–5.

[16] H. C. Lin, "Power harmonics and interharmonics measurement using recursive group-harmonic power minimizing algorithm," *IEEE Trans. Ind. Electron.*, vol. 59, no. 2, pp. 1184–1193, Feb. 2012.

[17] P. Drabek and M. Pittermann, "Calculation of interharmonics of power electronic converters – Using of harmonic analysis," *Ann. Faculty Eng. Hunedoara Int. J. Eng.*, Tome IX, Fascicule 1, pp. 151–154, 2011.

[18] A. Ramirez, "The modified harmonic domain: Interharmonics," *IEEE Trans. Power Del.*, vol. 26, no. 1, pp. 235–241, Jan. 2011.

[19] H. C. Lin, "Fast tracking of time-varying power system frequency and harmonics using iterative-loop approaching algorithm," *IEEE Trans. Ind. Electron.*, vol. 54, no. 2, pp. 974–983, Apr. 2007.

[20] M. Karimi-Ghartemani and M. R. Iravani, "Measurement of harmonics/inter-harmonics of time-varying frequencies," *IEEE Trans. Power Del.*, vol. 20, no. 1, pp. 23–31, Jan. 2005.

[21] M. Mojiri, M. Karimi-Ghartemani, and A. Bakhshai, "Processing of harmonics and interharmonics using an adaptive notch filter," *IEEE Trans. Power Del.*, vol. 25, no. 2, pp. 534–542, Apr. 2010.

[22] B. Chen, P. Li, G. Pin, and T. Parisini, "Estimation of multi-sinusoidal signals: A deadbeat methodology," in *Proc. IEEE Conf. Decis. Control*, Las Vegas, NV, USA, 2016, pp. 3763–3768.

[23] B. Chen, G. Pin, W. M. Ng, T. Parisini, and S. Y. R. Hui, "A fast-convergent modulation integral observer for online detection of the fundamental and harmonics in grid-connected power electronics systems," *IEEE Trans. Power Electron.*, vol. 32, no. 4, pp. 2596–2607, Apr. 2017.

[24] M. Albu and R. Popovici, "Rate of change of frequency – A power quality descriptor," in *Proc. IEEE Int. Conf. Harmonics Quality Power*, May 25–28, 2014, pp. 312–316.

[25] B. Chen, G. Pin, W. M. Ng, C. K. Lee, S. Y. R Hui, and T. Parisini, "An adaptive observer-based switched methodology for the identification of a perturbed sinusoidal signal: Theory and experiments," *IEEE Trans. Signal Process.*, vol. 62, no. 24, pp. 6355–6365, Dec. 2014.

[26] A. Testa *et al.*, "Interharmonics: Theory and modeling," *IEEE Trans. Power Del.*, vol. 22, no. 4, pp. 2335–2348, Oct. 2007.

[27] G. W. Chang, C. I. Chen, Y. J. Liu, and M. C. Wu, "Measuring power system harmonics and interharmonics by an improved fast Fourier transform-based algorithm," *IET Gener., Transmiss. Distrib.*, vol. 2, no. 2, pp. 192–201, 2008.

[28] J. R. de Carvalho, C. A. Duque *et al.*, "A PLL-based multirate structure for time-varying power systems harmonic/interharmonic estimation," *IEEE Trans. Power Del.*, vol. 24, no. 4, pp. 1789–1800, Oct. 2009.

[29] S.-W. Sohn, Y.-B. Lim, J.-J. Yun, H. Choi, and H.-D. Bae, "A filter bank and a self-tuning adaptive filter for the harmonic and interharmonic estimation in power signals," *IEEE Trans. Instrum. Meas.*, vol. 61, no. 1, pp. 64–73, Jan. 2012.

[30] H. Xue and P. Zhang, "Subspace-least mean square method for accurate harmonic and interharmonic measurement in power systems," *IEEE Trans. Power Del.*, vol. 27, no. 3, pp. 1260–1267, Jul. 2012.

[31] G. Betta, L. Ferrigno, and M. Laracca, "Cost-effective FPGA instrument for harmonic and interharmonic monitoring," *IEEE Trans. Instrum. Meas.*, vol. 62, no. 8, pp. 2161–2170, Aug. 2013.

[32] C.-I. Chen and Y.-C. Chen, "Comparative study of harmonic and interharmonic estimation methods for stationary and time-varying signals," *IEEE Trans. Ind. Electron.*, vol. 61, no. 1, pp. 397–404, Jan. 2014.

[33] Z. Sun, Z. He, T. Zang, and Y. Liu, "Multi-interharmonic spectrum separation and measurement under asynchronous sampling condition," *IEEE Trans. Instrum. Meas.*, vol. 65, no. 8, pp. 1902–1912, Aug. 2016.

[34] M. Hou, "Estimation of sinusoidal frequencies and amplitudes using adaptive identifier and observer," *IEEE Trans. Automat. Control*, vol. 52, no. 3, pp. 493–499, Mar. 2007.

[35] G. Pin, A. Assalone, M. Lovera, and T. Parisini, "Non-asymptotic kernel based parametric estimation of continuous-time linear systems," *IEEE Trans. Automat. Control*, vol. 61, no. 2, pp. 360–373, Feb. 2016.

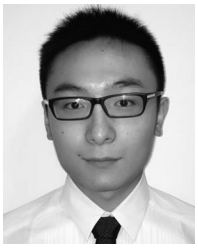

Boli Chen (M'16) received the B. Eng. degree in electrical and electronic engineering from Northumbria University, Newcastle upon Tyne, U.K., and Nanjing Normal University, Nanjing, China, in 2010, and the M.Sc. degree in control systems and the Ph.D. degree in control systems from Imperial College London, London, U.K., in 2011 and 2015, respectively.

Since 2015, he has been a Research Associate with Imperial College London, London, U.K. His research interests include nonlinear estimation and its application to sinusoidal identification and design of deadbeat identification algorithms and observers.

Gilberto Pin received the M.Sc. (*Laurea*) degree in electrical engineering (with honors) and the Ph.D. degree in information engineering, both from the University of Trieste, Trieste, Italy, in 2005 and 2009, respectively.

From 2009 to 2012, he was an Automation Engineer with Danieli Automation S.p.A., Italy. From 2013 to 2015, he was a Control Systems Engineer with the R&D Department, Electrolux Professional S.p.A., Italy. Since 2015, he has been an Energy Conversion Engineer with the Global Connectivity and Technology Center of Electrolux Major Appliances S.p.A., Italy. He is an author of several papers published in international conferences and scientific journals concerning control systems theory, signal processing methods, and control applications. His current research interests include nonlinear model predictive control, system's identification, finite-time observers, and industrial application of advanced control techniques.

Dr. Pin is a co-recipient of the IFAC Best Application Paper Prize of the *Journal of Process Control*, Elsevier, for the three-year period 2011–2013. Since 2012, he has been an Associate Editor for the Conference Editorial Board of the IEEE Control Systems Society. He is currently serving as an Associated Editor for the IEEE TRANSACTIONS ON CONTROL SYSTEMS TECHNOLOGY.

Wai Man Ng (M'04) received the B.Eng. degree in electronic engineering in 1998, the M.Phil. degree in electronic engineering from the City University of Hong Kong, Hong Kong, in 2004, and the Ph.D. degree in electronic engineering from the University of Hong Kong, Hong Kong, in 2015.

From 1998 to 2000, he was an Electronic Engineer with Astec Custom Limited. He was an Application Engineer with Ericsson Limited from 2000 to 2003. In 2009, he joined the City University of Hong Kong as a Research Fellow. Since 2011, he has been a Research Officer and the Laboratory Manager with the smart grid research facility Department of Electrical and Electronic Engineering, University of Hong Kong. He has authored or coauthored more than 20 journal and conference papers. He is the coinventor of two U.S. patents. His current research interests include electromagnetic interference, LED control, gas-discharge lamp, smart grid, and wireless power transfer.

Dr. Ng is a Chartered Engineer.

Peng Li received the B.Eng. degree in control technology and instruments in 2013 from Northeastern University, Shenyang, China, and the M.Sc. degree in control systems in 2014 from Imperial College London, London, U.K., where she is currently working toward the Ph.D. degree in control engineering.

Her research interests include finite-time system identification and estimation, design of fast fault detection, and isolation schemes.

Thomas Parisini (F'11) received the Ph.D. degree in electronic engineering and computer science from the University of Genoa, Genoa, Italy, in 1993.

Since 2001, he has been the Danieli Endowed Chair of Automation Engineering with the University of Trieste, Trieste, Italy. During 2009–2012, he was also the Deputy Rector for the University of Trieste. He was with Politecnico di Milano, and since 2010, he has been holding the Chair of Industrial Control and is the Director of Research with Imperial College London. He is the Deputy Director of the KIOS Research and Innovation Centre of Excellence, University of Cyprus, Nicosia, Cyprus. He has authored or coauthored more than 280 research papers in archival journals, book chapters, and international conference proceedings. His research interests include neural-network approximations for optimal control problems, fault diagnosis for nonlinear and distributed systems, nonlinear model predictive control systems, and nonlinear estimation.

Dr. Parisini is a co-recipient of the IFAC Best Application Paper Prize of the *Journal of Process Control*, Elsevier, for the three-year period 2011–2013 and of the 2004 Outstanding Paper Award of the IEEE TRANSACTIONS ON NEURAL NETWORKS. He is also a recipient of the 2007 IEEE Distinguished Member Award. In 2016, he became a Principal Investigator at Imperial of the H2020 European Union flagship Teaming Project KIOS Research and Innovation Centre of Excellence led by the University of Cyprus. In 2012, he was a recipient of an ABB Research Grant dealing with energy-autonomous sensor networks for self-monitoring industrial environments. He currently serves as the Vice President for Publications Activities of the IEEE Control Systems Society, and during 2009–2016 he was the Editor-in-Chief for the IEEE TRANSACTIONS ON CONTROL SYSTEMS TECHNOLOGY. Since 2017, he has been the Editor for control applications of *Automatica*. He is also the Chair of the IFAC Technical Committee on Fault Detection, Supervision and Safety of Technical Processes—SAFEPROCESS. He was the Chair of the IEEE Control Systems Society Conference Editorial Board and a Distinguished Lecturer of the IEEE Control Systems Society. He was an elected member of the Board of Governors of the IEEE Control Systems Society and of the European Control Association and a member of the board of evaluators of the 7th Framework ICT Research Program of the European Union. He is currently serving as an Associate Editor for the *International Journal of Control* and served as an Associate Editor for the IEEE TRANSACTIONS ON AUTOMATIC CONTROL, the IEEE TRANSACTIONS ON NEURAL NETWORKS, *Automatica*, and the *International Journal of Robust and Nonlinear Control*. Among other activities, he was the Program Chair of the 2008 IEEE Conference on Decision and Control and General Co-Chair of the 2013 IEEE Conference on Decision and Control. He is a Fellow of the IFAC.

Shu-Yuen Ron Hui (M'87–SM'94–F'03) received the B.Sc. (Eng. Hons.) degree in electrical and electronic engineering from the University of Birmingham, Birmingham, U.K., in 1984, and the D.I.C. and Ph.D. degrees in electrical engineering from Imperial College London, London, U.K., in 1987.

He is currently the holder of the Philip Wong Wilson Wong Chair Professorship with the University of Hong Kong, Hong Kong. Since July 2010, he has been concurrently held a part-time Chair Professorship of Power Electronics with Imperial College London. He has published more than 350 technical papers, including more than 250 refereed journal publications and book chapters. More than 60 of his patents have been adopted by industry. His inventions on wireless power underpin key features of the world's first wireless charging standard "Qi" with free positioning and localized charging.

Dr. Hui is an Associate Editor for the IEEE TRANSACTIONS ON POWER ELECTRONICS and the IEEE TRANSACTIONS ON INDUSTRIAL ELECTRONICS, and an Editor for the IEEE JOURNAL OF EMERGING AND SELECTED TOPICS IN POWER ELECTRONICS. He is the recipient of the 2010 IEEE Rudolf Chope R&D Award and the 2010 IET Achievement Medal (The Crompton Medal), and the 2015 IEEE William E. Newell Power Electronics Award. He is a Fellow of the Australian Academy of Technological Sciences and Engineering, and a Fellow of the Royal Academy of Engineering, U.K.